

# Variability study of the High Mass X-ray Binary IGR J18027–2016 with *Swift*–XRT

Nafisa Aftab<sup>1\*</sup>, Nazma Islam<sup>1,2</sup> and Biswajit Paul<sup>1</sup>

<sup>1</sup>Raman Research Institute, Sadashivnagar, Bangalore-560080, India

<sup>2</sup>Joint Astronomy Programme, Indian Institute of Science, Bangalore-560012, India

22 March 2021

## ABSTRACT

We report the results from pulsations and spectral analysis of a large number of observations of the HMXB pulsar IGR J18027–2016 with *Swift*–XRT, carried out at different orbital phases. In some orbital phases, as seen in different XRT observations, the X-ray intensity is found to vary by a large factor, of about  $\sim 50$ . In all the observations with sufficient number of source X-ray photons, pulsations have been detected around the previously known pulse period of  $\sim 140$  sec. When detected, the pulse profiles do not show any significant variation over a flux difference of a factor of  $\sim 3$ . The absorption column density is found to be large before and after the eclipse. We discuss various possible reasons for intensity and spectral variations in IGR J18027–2016, such as clumpy wind and hydrodynamic instabilities.

**Key words:** X-rays: stars - binaries: eclipsing - stars: neutron - X-rays: individual: IGR J18027–2016

## 1 INTRODUCTION

High Mass X-ray binary (HMXB) systems contain a companion star with mass  $\geq 10 M_{\odot}$  (either a main sequence star or a supergiant) and a compact object (either a neutron star or a black hole). Accretion onto the compact object occur via capture of stellar wind or Roche lobe overflow. HMXB systems are divided into two classes: (1) Be X-ray binary (Be HMXB) and (2) Supergiant X-ray binary (sgHMXB) some of which show the Supergiant Fast X-ray Transient (SFXT) Phenomena. Be HMXB and SFXTs are mostly transients in nature. In Be HMXBs, the accretion onto the compact object occurs via outflowing equatorial disk of the companion star stellar wind and the compact object passing through it (Reig 2011). Supergiant Fast X-ray Transients (SFXTs) are a sub class of HMXBs discovered with *INTEGRAL*, having recurrent, bright, short flares (Sguera et al. 2005), reaching  $L_X \sim 10^{36} - 10^{37}$  erg  $\text{sec}^{-1}$  (Sidoli et al. 2007), while their quiescent X-ray luminosity is  $\sim 10^{32}$  ergs  $\text{sec}^{-1}$  (Bozzo et al. 2010). Persistent sgHMXBs are found to have X-ray luminosity  $L_X = 10^{35} - 10^{36}$  ergs  $\text{sec}^{-1}$ , most of the time. Several short

off states have been observed in some of these systems: Vela X–1 – Manousakis & Walter (2015); Odaka et al. (2013); GX 301–2 – Göğüş, Kreykenbohm & Belloni (2011); 4U1907+09 – Doroshenko et al. (2012), 4U 1700–37 – Grebenev et al. (1999), OAO 1657–415 – Pradhan et al. (2014). On the other hand some sgHMXBs like SMC X-1 and LMC X-4 do not show off states, but they have strong short timescale flares (Moon, Eikenberry & Wasserman 2003; Moon & Eikenberry 2001). *INTEGRAL* observation of sgHMXBs show a wide range and type of intensity variation (Walter et al. 2015).

The HMXB IGR J18027–2016 was discovered with *INTEGRAL* – IBIS/ISGRI during the survey of the Galactic Center region in September 2003 (Revnivtsev et al. 2004). The pulsar is found to have a spin period of  $\sim 139$  sec (Iaria et al. 2004) and orbital period of 4.57 days (Hill et al. 2005; Jain, Paul & Dutta 2009) around a supergiant companion with spectral type B1-Ib (Torrejón et al. 2010). Hill et al. (2005) characterised the combined *XMM-Newton* and *INTEGRAL* X-ray spectrum of the pulsar by a broken power law, modified by a photoelectric absorption along the line of sight hydrogen column density  $N_H \sim 10^{23}$   $\text{cm}^{-2}$ . A soft excess is also detected in the spectra of this source (Hill et al. 2005; Walter et al. 2006).

In this work, we have analyzed all *Swift*–XRT obser-

\* E-mail: nafisa@rri.res.in

vations of IGR J18027–2016 to investigate its long term pulsation and spectral characteristics. We searched for pulsations in all the observations and folded the light-curves with the estimated pulse period to study its pulse profiles. Orbital intensity analysis show some low X-ray intensity episodes of the source, similar to that seen in Vela X–1, GX 301–2, 4U 1907+09 (Manousakis & Walter 2015; Göğüş, Kreykenbohm & Belloni 2011; Doroshenko et al. 2012), OAO 1657–415 (Barnstedt et al. 2008) etc. We have further investigated the nature of the system by studying its spectral characteristics at different orbital phases. Our results can put some useful insight into systems having sudden off states in X-ray intensity.

## 2 DATA AND ANALYSIS

*Swift* observatory was launched in November 2004 (Gehrels et al. 2004), consisting of 3 sets of instruments: 1) Burst Alert Telescope (BAT), operating in the energy range of 15–150 keV (Barthelmy et al. 2005) 2) X-ray Telescope (XRT), operating in the range of 0.2–10 keV (Burrows et al. 2007) 3) Ultraviolet and Optical Telescope (UVOT), having UV and optical coverage of 170–600 nm (Roming et al 2005). XRT and UVOT are two narrow field instruments, coaligned and pointed to the center of FOV of BAT.

BAT is a coded aperture instrument with CdZnTe detector, having a field of view  $100^\circ \times 60^\circ$  and a detection sensitivity of 5.3 mCrab (Krimm et al. 2013). XRT is a focusing telescope which employs an X-ray CCD detector with a Wolter 1 mirror set of 3.5 m focal length, with  $23.6 \times 23.6$  arcmin FOV. The imaging array consists of  $600 \times 600$  image pixels, each with  $40 \mu\text{m} \times 40 \mu\text{m}$  size and 2.5 arcsec/pixel resolution. It operates on 3 read-out modes namely Imaging (IM), Windowed Timing (WT) and Photon Counting (PC) mode with few sub modes. In Imaging mode (IM), image of the object is obtained by CCD read-out. Photons are allowed to pile up and photon recognition is not done in this mode. Windowed timing mode (WT) produces 1.7 ms resolution timing with 1D position information and full energy resolution for flux less than 600 mCrab. Photon counting mode (PC) contributes to full imaging and spectroscopic resolution with time resolution of 2.6 sec.

We have analyzed 33 separate *Swift*–XRT observations of IGR J18027–2016 from MJD 54141 to 56171. We have also used  $\sim 10.5$  years of *Swift*–BAT lightcurve to make an accurate estimation of the orbital period of this system.<sup>1</sup> Minimum exposure time amongst 33 *Swift*–XRT observations  $\sim 300$  sec and maximum exposure  $\sim 10$  kilosec. We used Photon Counting (PC) mode data, because 32 observations out of 33 had only this datamode. We filtered level1 data with the task XRTPIPELINE and obtained cleaned event files for all observations. For the barycenter correction of the time column of the event files we used the FTOOL BARYCORR. We extracted the source photons from a region with  $60''$  radius centering

the source and the background photons from a similar region in the FOV that is free of any other X-ray sources. We used these source and background region files to extract corresponding lightcurves and spectra using XSELECT v2.4C.

We have generated exposure maps with the task XRTEXT-POMAP to correct for the loss of flux due to some hot CCD pixels. We then used this exposure map to create ancillary file with the routine XRTMKARF which was then used for the spectral fitting in XSPEC. We obtained the response file from the latest *Swift* calibration dataset CALDB v1.3.0. For 5 observations, the source could not be distinctly identified from the background, even with the task XRTCENTROID. For these observations, we extracted the lightcurves and spectra with region files centered at the R.A.(18h 02m 41.94s) and Dec.( $-20^\circ 17' 17.3''$ ) of the source (Torrejón et al. 2010). Observation at MJD 54141 was longer in duration ( $\sim 10$  ks) and observations at MJD 56085 and 56096 showed significant difference in the count rate at the beginning and end of the observation. So we divided lightcurves and spectra of these three observations into two parts to investigate them separately. Therefore, we have total 36 separate lightcurves and spectra to carry out timing and spectral analysis.

### 2.1 Pulsation Analysis

We searched for pulsations with the FTOOL task EFSEARCH for all the observations in which the source is clearly visible in the image and the total number of source photons were more than 600. EFSEARCH results of all these lightcurves gave a maximum  $\chi^2$  of greater than 100 for 32 phasebins per period indicating a clear detection of the X-ray pulses. Table 1 shows the exposure time, total number of photons in  $60''$  source region, average count rate, pulse period and orbital phase of all observations, along with the observations which were divided into two parts mentioned in Section 2, arranged in the ascending order of the total number of source photons.

Light curve of each observations with pulsation detected were folded with corresponding pulse periods. Folded pulse profile of the 15 observations with pulsation detected are shown in Figure 1. The pulse profiles have been aligned such that the phase of the main peak of each profile lies at 1.0. As seen in Figure 1, most of the pulse profiles show a double peaked structure, with a possible indication of variation in relative intensity of the peaks. Only for the purpose of comparing the strengths of the two peaks, we fitted each of these pulse profiles with two gaussian, one for the primary pulse and the other for the secondary along with an unpulsed component. We define pulse fraction of the two peaks as the fractional area of the two gaussians. We obtained pulse fraction for both the peaks and plotted them in the top panel of Figure 2 along with their ratio i.e. the relative pulse fraction of the secondary to the primary in the bottom panel as function of flux. We see that while the overall pulse fraction has a weak negative correlation with the flux, the relative pulse fraction of the two peaks is nearly constant.

<sup>1</sup> <http://swift.gsfc.nasa.gov/results/transients/weak/IGRJ18027-2016>

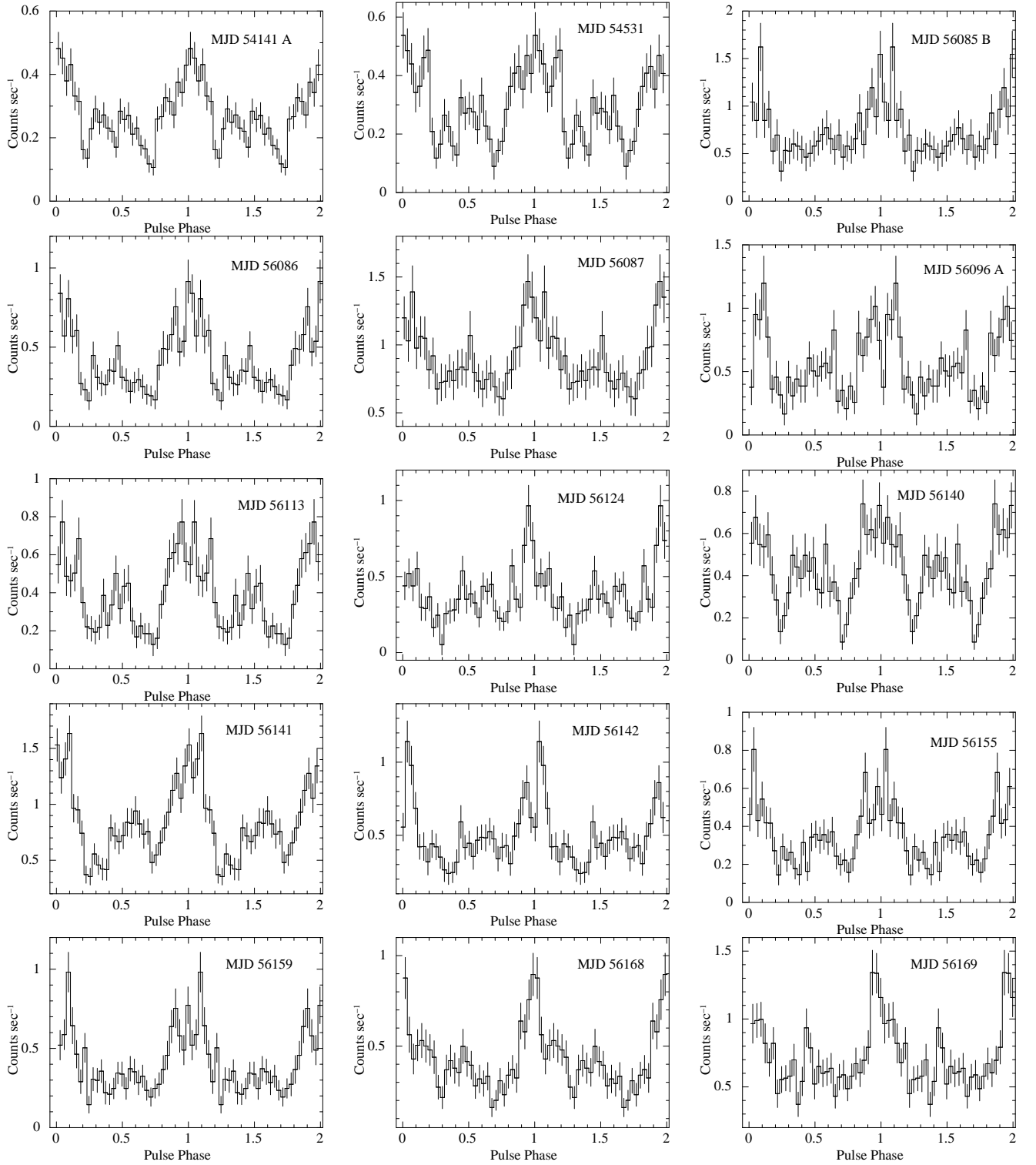


**Figure 1.** Pulse profiles of 15 observations with clear detection of pulsation, folded with their estimated pulse periods and with 32 phasebins/period. Main peaks of all the profiles have been aligned at phase 1.0. The MJD of each observations are labelled inside each panel.

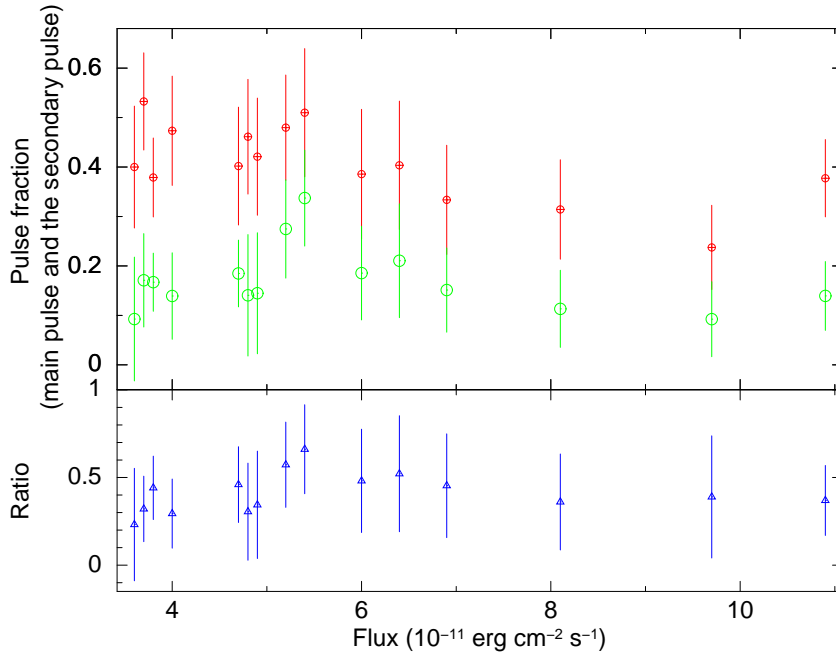


**Figure 2.** Top panel: Pulse fraction of the main or primary (red) and secondary pulse (green) plotted as function of flux. Bottom panel: Ratio of the pulse fraction of the primary to the secondary pulse fraction plotted as function of flux.

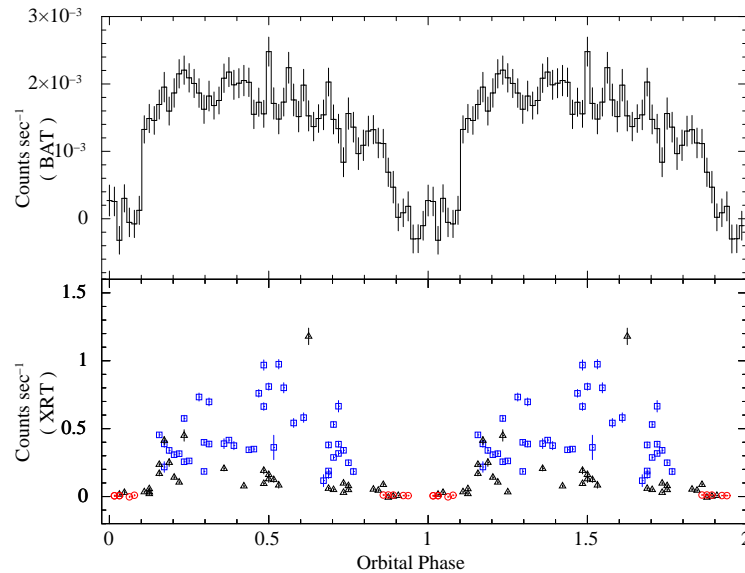


**Figure 3.** Top panel: Orbital intensity profile of IGR J18027–2016 obtained by folding *Swift*–BAT light-curve with orbital period of 394843 sec. Bottom panel: *Swift*–XRT lightcurves modulo same orbital period in three colours: pulsation detected where number of source photons is greater than 600 – blue, number of source photons is less than 600 – black; faint – red.

## 2.2 Orbital period analysis

We have searched for orbital period in the *Swift*–BAT light curve with the FTOOL task EFSEARCH and found it to be 394843 sec (4.57 days; similar to  $P_{orb}$  determined by Hill et al. 2005; Jain, Paul & Dutta 2009). We then folded the *Swift*–

BAT lightcurve with this orbital period, and in the folded profile (shown in the top panel of Figure 3), we can see an eclipse for duration of nearly  $\frac{1}{4}$ th of the orbital period. In the bottom panel of Figure 3, we have plotted the orbital phase-wise X-ray count-rates obtained from all *Swift*–XRT lightcurves in three colours: pulsation detected where source photon is

**Table 1.** Log of observations with exposure time, total number of source photons, average count-rate, pulse period and orbital phase. A and B refers to the observations which were split as mentioned in Section 2.

Observation MJD	Observation ID	Exposure time (sec)	Total no of photons in source region	Average count-rate (counts/sec)	Pulse Period (sec)	Orbital Phase
56143	00035720023	929	6	0.01	-	0.02 - 0.03
56098	00035720011	874	8	0.01	-	0.06 - 0.08
56085 A	00035720005 A	442	16	0.04	-	0.13
56171	00035720034	2025	22	0.01	-	0.92 - 0.94
56144	00035720024	2093	26	0.01	-	0.02 - 0.03
56125	00035720017	2035	29	0.01	-	0.86 - 0.89
56089	00035720009	989	42	0.04	-	0.25
56157	00035720027	1913	50	0.03	-	0.03 - 0.05
56156	00035720026	2035	81	0.04	-	0.73 - 0.75
56167	00035720030	1975	99	0.05	-	0.11 - 0.13
56170	00035720033	1988	126	0.06	-	0.69 - 0.70
55751	00035720004	692	127	0.18	-	0.16
54141 B	00035720001 B	3798	142	0.03	-	0.83 - 0.91
56128	00035720019	1231	180	0.15	-	0.48 - 0.53
56088	00035720008	2020	204	0.10	-	0.73 - 0.75
56118	00035720015	1878	218	0.12	-	0.48 - 0.5
56126	00035720018	1898	252	0.13	-	0.20 - 0.22
56100	00035720013	2170	282	0.13	-	0.36 - 0.42
56158	00035720028	1523	376	0.25	-	0.16
56096 B	00035720010 B	327	415	1.18	-	0.63
56099	00035720012	1121	417	0.39	-	0.17 - 0.23
56096 A	00035720010 A	1059	620	0.56	140.12±0.01	0.58 - 0.61
56085 B	00035720005 B	852	699	0.73	141.31±0.01	0.28
56113	00035720014	1920	719	0.41	139.69±0.01	0.30 - 0.31
56155	00035720025	2143	772	0.36	140.01±0.01	0.44 - 0.45
56124	00035720016	1855	780	0.42	143.35±0.01	0.69 - 0.72
56086	00035720006	1873	796	0.43	139.75±0.01	0.30 - 0.31
56159	00035720029	1968	822	0.42	140.01±0.01	0.36 - 0.39
56140	00035720020	1955	876	0.45	139.66±0.01	0.16 - 0.17
56168	00035720031	2038	900	0.44	140.14±0.01	0.23 - 0.25
54531	00035720002	2914	909	0.31	139.66±0.01	0.17 - 0.23
56142	00035720022	1960	1035	0.53	139.48±0.01	0.69 - 0.72
56087	00035720007	1446	1329	0.92	143.25±0.01	0.53 - 0.55
56169	00035720032	1865	1370	0.74	140.20±0.01	0.47 - 0.48
54141 A	00035720001 A	5789	1617	0.27	139.95±0.01	0.67 - 0.77
56141	00035720021	1970	1729	0.88	139.87±0.01	0.48 - 0.52

greater than 600 – blue; source photon less than 600 – black; faint, i.e. where source could not be seen clearly – red. To investigate any intensity variations other than the long time averaged orbital intensity modulation, multiple observations with *Swift*-XRT during the same orbital phase range are not averaged here, unlike the orbital profile shown in Figure 3 in Bozzo et al. (2015).

In Figure 3, the bottom panel shows the variability in count-rate of the source in the orbital intensity profile with the pointed *Swift*-XRT observations, whereas the *Swift*-BAT orbital intensity profile is averaged over many orbital cycles, indicating a sub-orbital variability similar to that seen in IGR J16393-4643 (Islam et al. 2015) and OAO 1657–415

(Pradhan et al. 2014; Barnstedt et al. 2008). Around orbital phase 0.5, there are multiple *Swift*-XRT observations showing significant difference in the count rates. We have shown spectra and lightcurve for two parts of observations carried out in same orbital phase ranges (0.48-0.52, 0.69-0.75) in Figure 4. The light curve is binned with 140 seconds (close to the spin period of the pulsar) to avoid seeing any effect of the pulse profile related variation in the light curve. In the top panel in Figure 4 there are about 140 photons per bin and the variability in the light curves is clearly larger than the photon noise (represented by the  $1\sigma$  error bars in each bin). The number of counts per bin in the two light curves shown in the middle panel is smaller and have correspondingly larger

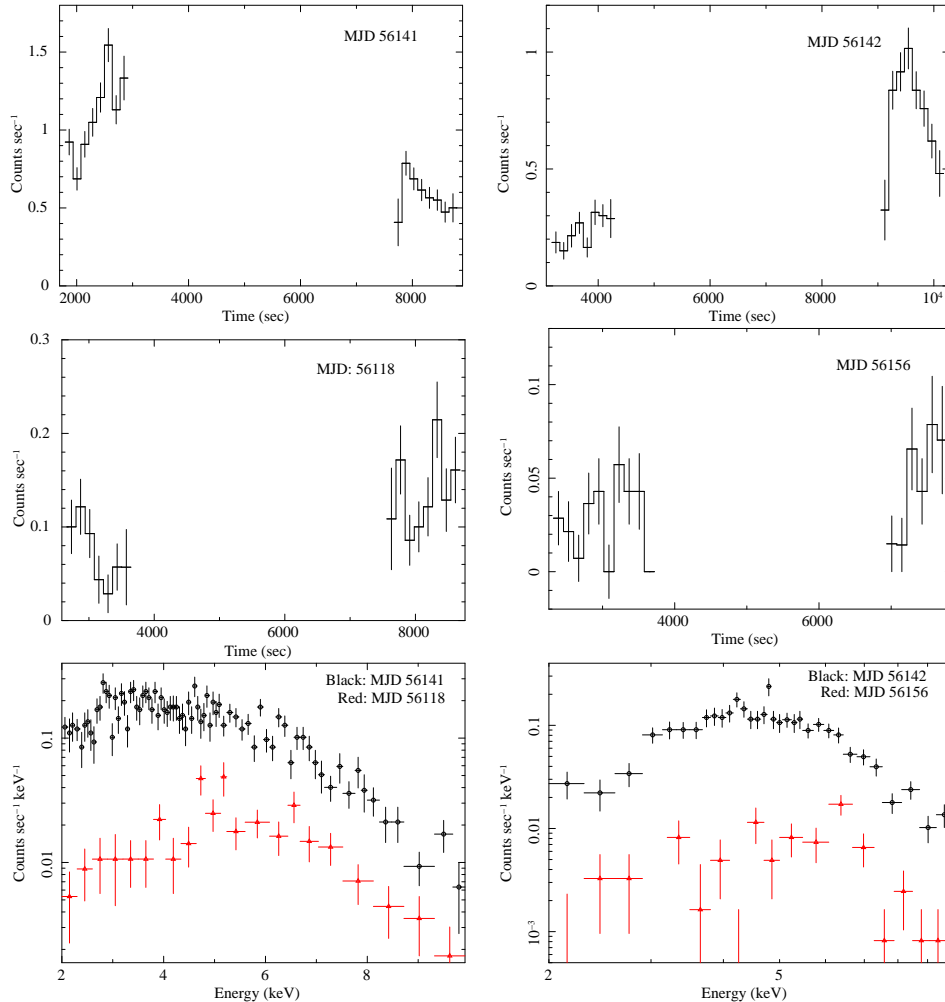


**Figure 4.** *Left panel:* The top and middle panel show the light-curves of two observations centered at orbital phase 0.48–0.52. In the top panel, the light-curve of an observation (MJD 56141) shows a high count-rate whereas the middle panel shows another observation (MJD 56118) in the same orbital phase range, having a low count-rate. The lower panel is the plot of spectra of these two observations which bring out the fact that in the same orbital phase range, the X-ray intensities vary by a factor of  $\sim 10$ . *Right panel:* Same is shown for another set of observations (MJD 56142 and MJD 56156) centered at orbital phase range 0.69–0.75, but showing a large change in X-ray intensities.

uncertainties. No intensity variation can be ascertained in the light curves shown in the middle panels. Spectra of these two observations are shown in the lower panel of Figure 4 which bring out the fact that in the same orbital phase range, the X-ray intensities vary by a factor of  $\sim 10$ .

### 2.3 Spectral Analysis

We fitted X-ray spectrum for 21 observations, having moderate statistics, using XSPEC v12.8.2 in the energy range 2.0–9.0 keV. Because of limited statistics. The spectra were modelled with a power law modified by a photoelectric absorption by column density of absorbing matter along our line of sight. We have also fitted the spectra from the remaining observations only for the purpose of estimating the total flux. We have found the equivalent column density of hydrogen ( $N_H$ )

in the range of  $10^{22}$ – $10^{23}$  cm<sup>-2</sup>. We have plotted two spectra in Figure 5 obtained at MJD 56086 and 56126 to show the variation in the absorption at low energies. The spectra clearly indicate large difference in column density. Flux during the out-of-eclipse orbital phase are found to be in the range of  $(0.4\text{--}14) \times 10^{-11}$  ergs cm<sup>-2</sup> sec<sup>-1</sup>. We have plotted the spectral parameters  $N_H$ ,  $\Gamma$  and total flux (2.0–9.0 keV) from the system in Figure 6.

## 3 DISCUSSION

In this work, we have analyzed all available *Swift*-XRT observations of the HMXB source IGR J18027–2016, to study its pulsations and variability characteristics. Pulsations have been detected in all the observations having a total number

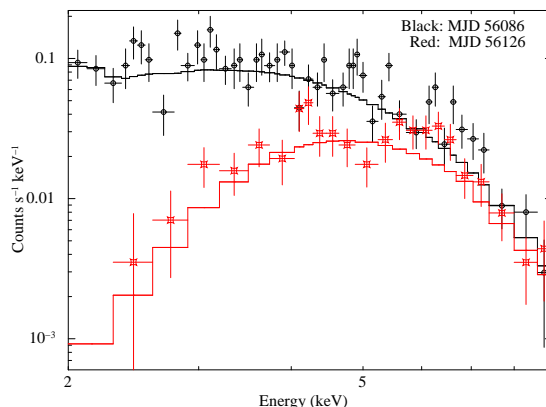


**Figure 5.** Spectra at MJD 56086 AND 56126 are plotted together to show the variation in low energy absorption

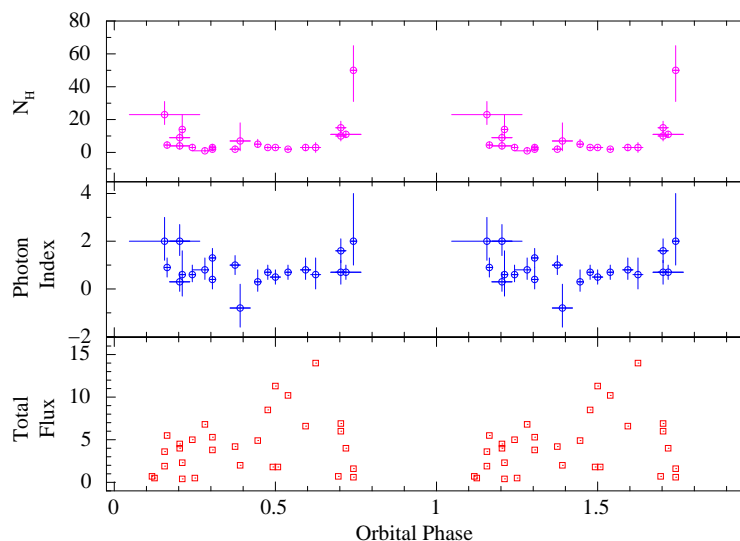


**Figure 6.** Variation of column density of hydrogen ( $N_H$  in units of  $10^{22} \text{cm}^{-2}$ ), photon index ( $\Gamma$ ), total flux ( $F$  in the units of  $10^{-11} \text{ergs.cm}^{-2}\text{sec}^{-1}$ ).

of source photons greater than 600 (Table 1) and the light-curves of these observations were folded with the pulse periods to create pulse profiles (Figure 1). Some of the pulse profiles are found to have double peaked structure. We therefore carried out an analysis of the pulse profile and determined the pulse fractions of the two peaks. We have plotted these pulse fractions and their ratio (primary pulse fraction to the secondary) in Figure 2 as function of flux and find no evidence for significant variation in the pulse profiles over a factor  $\sim 3$  variation in flux.

The pulse profiles of accreting X-ray pulsars show strong energy dependence (Nagase 1989), usually having simpler pulse profile at higher energies ( $>10$  keV) and complex profile at low energies, often resulting due to phase locked absorption. However in a given energy band, most persistent HMXB pulsars *i.e* sources with supergiant companion have pulse profiles that are stable over long periods of time (Vela X-1 – Kreykenbohm et al. 1999, Maitra & Paul 2013).

The transient pulsars, on the other hand, show very strong time/luminosity dependence of the pulse profile, which can be attributed to the changes in the structure of the X-ray emission region (accretion column) during the transient phase (Devasia et al. 2011). The limited pulse profile changes in IGR J18027–2016 is consistent with other persistent HMXBs.

The long term averaged orbital intensity profile of this source created with *Swift*-BAT light-curves is smoothly varying, having an eclipse lasting for about 1/4 th of the orbit (top panel of Figure 3). The *Swift*-XRT and *INTEGRAL* light-curves, when averaged also give smoothly varying orbital intensity profiles (Bozzo et al. 2015; Hill et al. 2005). However, the *Swift*-XRT light-curves, when plotted individually for all the observations as a function of orbital phase, shows a significant count-rate variation outside the eclipse (bottom panel of Fig 3). Within the same observation carried out around orbital phase 0.3-0.5 (MJD: 56085), the X-ray count-rates are found to vary by a fac-

tor of 36. A maximum count-rate variation (a factor of 48) is shown by two non-eclipse observations at MJD 56085 and MJD 56087. These short term variation could also be due to hydrodynamical instabilities. Manousakis & Walter (2015) has produced the hard X-ray variation observed with INTEGRAL-ISGRI and RXTE-PCA with hydrodynamical instabilities predicted by simple model without considering intrinsic clumping or propeller effect. In some cases like in OAO 1657–415, the variations in X-ray intensity may also arise due to the accretion onto the compact object by inhomogeneous clumpy winds (Oskinova, Feldmeier & Kretschmar 2013; Pradhan et al. 2014; Barnstedt et al. 2008).

In the present work, we detect several low X-ray intensity episodes (For *e.g.* in orbital phases 0.5 and 0.7) in the supergiant HMXB IGR J18027–2016, indicating these episodes to be either off-states like episode similar to Vela X–1 (Doroshenko, Santangelo & Suleimanov 2011) or possibly the presence of clumpy wind like OAO 1657–415 (Pradhan et al. 2014; Barnstedt et al. 2008). From these XRT observations, we cannot distinguish from either of these two or other scenarios.

X-ray spectra were extracted for 21 *Swift*–XRT observations, having moderate statistics to fit with a simple power-law model, modified for photo-electric absorption. spectra of other observations with limited statistics were also fitted with the same models just for the purpose of estimating total flux. The value of absorption column density  $N_H$  is as high as  $5 \times 10^{23} \text{ cm}^{-2}$ , which is similar to the values obtained by Hill et al. (2005); Walter et al. (2006), and indicate a dense circumstellar environment around the neutron star. From Figure 6, we see an increase in  $N_H$  just before and after the eclipse, similar to that seen in 4U 1538–52 (Rodes-Roca et al. 2015; Mukherjee et al. 2006).

IGR J18027–2016 presents an interesting case of a supergiant source showing evidence of low X-ray intensity states, similar to well known sources like Vela X-1. Detailed X-ray timing and spectroscopic observations of IGR J18027–2016 at various orbital phases with other X-ray missions would be useful to understand the nature of these low intensity states.

#### ACKNOWLEDGEMENT

We thank the referee Roland Walter for suggestions that helped us to improve the paper. The data used for this work has been obtained through the High Energy Astrophysics Science Archive (HEASARC) On-line Service provided by NASA/GSFC. We have also used the public light-curves from *Swift*–BAT site.

#### REFERENCES

- Barnstedt J. et al., 2008, *A&A*, 486, 293  
 Barthelmy S. D. et al., 2005, *Space Sci. Rev.*, 120, 143  
 Bozzo E., Romano P., Ducci L., Bernardini F., Falanga M., 2015, *Advances in Space Research*, 55, 1255  
 Bozzo E., Stella L., Ferrigno C., Giunta A., Falanga M., Campana S., Israel G., Leyder J. C., 2010, *A&A*, 519, A6  
 Burrows D. N. et al., 2007, in *Society of Photo-Optical Instrumentation Engineers (SPIE) Conference Series*, Vol. 6686, *Society of Photo-Optical Instrumentation Engineers (SPIE) Conference Series*, p. 7  
 Devasia J., James M., Paul B., Indulekha K., 2011, *MNRAS*, 417, 348  
 Doroshenko V., Santangelo A., Ducci L., Klochkov D., 2012, *A&A*, 548, A19  
 Doroshenko V., Santangelo A., Suleimanov V., 2011, *A&A*, 529, A52  
 Gehrels N. et al., 2004, *ApJ*, 611, 1005  
 Göğüş E., Kreykenbohm I., Belloni T. M., 2011, *A&A*, 525, L6  
 Grebenev S. A., Lyashenko O. V., Pavlinsky M. N., Sunyaev R. A., 1999, *Astrophysical Letters and Communications*, 38, 89  
 Hill A. B. et al., 2005, *A&A*, 439, 255  
 Iaria R., Augello G., Robba N. R., di Salvo T., Burderi L., Lavagetto L., 2004, in *Revista Mexicana de Astronomia y Astrofisica*, vol. 27, Vol. 20, *Revista Mexicana de Astronomia y Astrofisica Conference Series*, Tovmassian G., Sion E., eds., pp. 212–212  
 Islam N., Maitra C., Pradhan P., Paul B., 2015, *MNRAS*, 446, 4148  
 Jain C., Paul B., Dutta A., 2009, *Research in Astronomy and Astrophysics*, 9, 1303  
 Kreykenbohm I., Kretschmar P., Wilms J., Staubert R., Kendziorra E., Gruber D. E., Heindl W. A., Rothschild R. E., 1999, *A&A*, 341, 141  
 Krimm H. A. et al., 2013, *ApJS*, 209, 14  
 Maitra C., Paul B., 2013, *ApJ*, 763, 79  
 Manousakis A., Walter R., 2015, *A&A*, 575, A58  
 Moon D.-S., Eikenberry S. S., 2001, *ApJ*, 549, L225  
 Moon D.-S., Eikenberry S. S., Wasserman I. M., 2003, *ApJ*, 582, L91  
 Mukherjee U., Raichur H., Paul B., Naik S., Bhatt N., 2006, *Journal of Astrophysics and Astronomy*, 27, 411  
 Nagase F., 1989, *PASJ*, 41, 1  
 Odaka H., Khangulyan D., Tanaka Y. T., Watanabe S., Takahashi T., Makishima K., 2013, *ApJ*, 767, 70  
 Oskinova L. M., Feldmeier A., Kretschmar P., 2013, in *IAU Symposium*, Vol. 290, *IAU Symposium*, Zhang C. M., Belloni T., Méndez M., Zhang S. N., eds., pp. 287–288  
 Pradhan P., Maitra C., Paul B., Islam N., Paul B. C., 2014, *MNRAS*, 442, 2691  
 Reig P., 2011, *Ap&SS*, 332, 1  
 Revnivtsev M. G. et al., 2004, *Astronomy Letters*, 30, 382  
 Rodes-Roca J. J., Mihara T., Nakahira S., Torrejón J. M., Giménez-García Á., Bernabéu G., 2015, *A&A*, 580, A140  
 Sguera V. et al., 2005, *A&A*, 444, 221  
 Sidoli L., Romano P., Mereghetti S., Paizis A., Vercellone S., Mangano V., Götz D., 2007, *A&A*, 476, 1307  
 Torrejón J. M., Negueruela I., Smith D. M., Harrison T. E.,



2010, A&A, 510, A61  
Walter R., Lutovinov A. A., Bozzo E., Tsygankov S. S., 2015,  
ArXiv e-prints  
Walter R. et al., 2006, A&A, 453, 133